

International Conference on Space Optics—ICSO 2018

Chania, Greece

9–12 October 2018

Edited by Zoran Sodnik, Nikos Karafolas, and Bruno Cugny



How effective is tip-tilt pre-compensation for optical uplinks based on the received downlink optical signal?

D. Alaluf

J. Perdigues Armengol

Z. Sodnik



How effective is tip-tilt pre-compensation for optical uplinks based on the received downlink optical signal?

D. Alaluf^{*a}, J. M. Perdigues Armengol^a, Z. Sodnik^a

^a European Space Agency (ESA)
European Space Technology and Research Centre (ESTEC)
2200AG Noordwijk, The Netherlands

Email: david.alaluf@esa.int

Email: josep.maria.perdigues.armengol@esa.int

Email: zoran.sodnik@esa.int

ABSTRACT

This paper investigates the effectiveness of pre-compensating the beam wander effect (tip-tilt distortion) experienced by an uplink optical signal, from a ground station to a satellite, based on the tip-tilt information of the downlink signal (from the satellite to the ground). A test campaign was carried out in May 2018 at the Optical Ground Station (OGS) of the European Space Agency (ESA), to perform measurements of double stars featuring angular separations representative of the point-ahead angle of GEO/LEO satellites. The purpose of gathering these measurements is to investigate the relationship between double stars angular separation and their differential tip-tilt distortion. This analysis evaluates the influence of the point-ahead angle of the satellite, on the tip-tilt correlation between the uplink and the downlink signals. This paper describes the algorithm used to determine the tip-tilt error due to anisoplanatism, and presents the preliminary results that were extracted from the measurements. Then, it is shown how to estimate the jitter of the telescope from the common motion of two independent stars as seen in the focal plane of the telescope. Finally, the paper provides a methodology to determine the maximum transmitter aperture diameter of a ground-based laser communication terminal, in case tip-tilt pre-compensation is applied to the uplink signal based on the received satellite signal.

Keywords: laser communications; free-space optical communications; laser communications terminal; ground to space communications; tip-tilt pre-compensation, adaptive optics; anisoplanatism; isoplanatic angle; atmospheric turbulence; optical ground station

1. INTRODUCTION

Over the last few years, optical links between satellites and Earth have become more and more popular in response to a growing demand for high-speed communications terminals. Optical communications is of particular interest, with respect to radio frequency communications, in terms of available bandwidth, low mass, low volume, power consumption and data transfer security. Furthermore, no frequency license is required to operate optical communications since laser beams do not lead to interferences between different data links [1]. Nevertheless, eye safety regulation does apply to laser-based communication systems and it needs to be carefully considered during the design phase.

Despite its great potential, some challenging aspects need to be addressed to exploit this promising technology. Indeed, laser-based communications suffer multiple distortions when crossing the atmosphere. One of the most noticeable impairments is caused by the fact that the atmosphere is continuously and randomly deviating the beam of light from its original direction, so called “beam wander effect”. These distortions not only impact the Bit Error Ratio (BER) of the system but can even make the link unfeasible [2].

A pre-distortion (i.e. tip-tilt pre-compensation) of the signal emitted by an optical ground station towards GEO/LEO satellites can be considered, so as to pre-compensate the beam wander induced by the atmosphere. In cases of small point-ahead angle (typically 4 arcsec for GEO satellites), the received signal from the satellite may be used as a reference to determine the amount of correction to apply to the uplink optical signal. However, in other scenarios, the received signal may not be used to pre-distort the outgoing signal because the angular separation between the incoming and the outgoing signals is so large that the turbulence effects in both directions are uncorrelated (i.e., the point-ahead angle is much larger than the tilt isoplanatic angle see section 2). In this paper, we propose to investigate the tip-tilt correlation between signals received from two independent stars featuring an angular separation similar to the required point-ahead angle for different optical link scenarios between space and Earth. This makes it possible to evaluate the effectiveness of a tilt pre-compensation based on the signal received from the satellite, with respect to the angular separation between the downlink and the uplink signals. A similar study has been conducted in [3]; the authors estimated the correlation between the downlink path of a natural guide star (NGS) and a laser guide star (LGS), with respect to their angular separation. Conversely, in the present paper, the measurements have been performed using double stars only. In this framework, a test campaign was carried out in May 2018, at ESA's Optical Ground Station (in Tenerife); the present paper reports on the preliminary results that were extracted from the measurements, and compares them to a theoretical model. It is then shown how these measurements were used to evaluate the jitter of the telescope and to help dimensioning the ground-based transmitter aperture diameter.

The paper is organized as follows: section 2 gives a brief theoretical introduction, section 3 describes the measurement setup, section 4 introduces the algorithm used to calculate the centroids of the double stars, and presents the preliminary results; section 5 evaluates the jitter of the 1-m telescope used for the measurements; finally, section 6 assesses the impact of applying tip-tilt pre-compensation to the uplink signal based on the received satellite signal, for LEO and GEO to ground communication scenarios.

2. THEORETICAL BACKGROUND

2.1. ATMOSPHERIC TURBULENCE PROFILE

For a given site and at a particular time, the atmospheric turbulence is described by the so-called refractive-index structure, $C_n^2(h)$, which characterize the strength of the turbulence with respect to the altitude, h , in the atmosphere. Since the atmosphere is denser at low altitudes, the contribution of the low-altitude layers are generally rather important.

Several models have been proposed to describe the behaviour of the atmosphere (depending on the location of the observatory, the number of turbulence layers considered, the importance given to each layer etc.). Among them, the Hufnagel-Valley profile (HV) [4] is the most commonly used but is only valid at sea level. Given that the Optical Ground Station (OGS) is located at $H_{OGS} = 2393$ meters over the sea, modification to the atmospheric model are necessary. Just truncating the HV model would lead to an underestimation of the turbulence strength. Therefore, a modification of the model is used to consider the ground station altitude. This model is called the modified Hufnagel-Valley (MHV) and is given by the following equation [5]:

$$C_n^2(h) = 0.00594 \left(\frac{v}{27}\right)^2 (10^{-5}h)^{10} e^{-h/1000} + 2.710^{-16} e^{-h/1500} + A_0 e^{-H_{OGS}/700} e^{-(h-H_{OGS})/100} \quad (1)$$

where v stands for the RMS cross wind velocity, and A_0 is a reference sea-level turbulence value for scaling according to day- and night-time. Note that this model is defined for $h > H_{OGS}$. In this paper, these parameters have been set to $A_0 = 6 \cdot 10^{-16} m^{-2/3}$ and $v = 21 m/s$ as suggested in [5] for the OGS. It is worth mentioning that such a simple empirical model gives an order of magnitude of the expected turbulence and may be rather inaccurate because it does not account for instantaneous meteorological conditions, local topographic characteristics nor seasonal influences.

2.2. BEAM WANDER

The beam wander is due to large-scales turbulence structures, appearing close to the ground, resulting in random fluctuations of the beam path with respect to its initial direction. This phenomenon is even more critical for optical uplinks since atmospheric turbulence happens close to the Earth's surface where small angular deviations can lead to large pointing errors (beam displacement up to several hundred meters). Since the beam size is often smaller than typical turbulence eddy size, the beam wander is a major concern for optical communications. The standard deviation of the beam wander is given by [6]:

$$\sigma_{BW} \approx 0.73 \left(\frac{\lambda}{2W_0} \right) \left(\frac{2W_0}{r_0} \right)^{\frac{5}{6}}, \quad (2)$$

where λ is the operating wavelength, W_0 is the initial beam radius, r_0 is the Fried parameter (i.e the atmospheric-coherence length) and is given by [7]:

$$r_0 = 0.185 \lambda^{6/5} \left[\sec(\gamma) \int_0^\infty C_n^2(h) dh \right]^{-3/5}, \quad (3)$$

where γ is the zenith angle. Observe that since r_0 is proportional to $\lambda^{6/5}$, σ_{BW} is constant regardless of the wavelength. The previous equation shows that the Fried parameter decreases as the zenith angles increases. This means that the wavefront can be considered as coherent over a smaller area at low elevations than for elevations close to the zenith. This in turn implies that the beam wander is more important at low elevations.

It is also worthwhile to point out that diffraction causes the diameter, D , of a collimated beam to increase in size over distance according to the beam divergence angle:

$$\Phi \propto \frac{\lambda}{D} \quad (4)$$

Therefore, if the beam wander is larger than the divergence of the beam, Φ , strong fading will occur.

Eq. (2) shows that large diameter transmitters are slightly less impacted by beam wander than small apertures. However, one observe from Eq. (4) that the divergence experienced by a beam decreases with the increase of the transmitter aperture, which makes the optical link much more sensitive for large diameter transmitters. On the other hand, small aperture transmitters involve large divergence, hence large power loss, but are more robust against beam wandering.

2.3. POINT-AHEAD ANGLE AND ISOPLANATIC ANGLE

Due to the relative motion between the satellite and the ground station, the returned signal (i.e from Earth to the satellite) needs to be angularly offset in order to reach the satellite. This pointing offset is called the point-ahead angle and depends exclusively on the differential velocity between the two communicating parties perpendicular to their line of sight. The point-ahead angle can range between few arcseconds (typically 4 arcsec for GEO satellites) up to ~10 arcseconds for LEO satellites.

The isoplanatic angle corresponds to the angle over which the atmospheric turbulence can be considered as unchanged. Therefore, the larger the isoplanatic angle, the better is the pre-compensation based on the downlink signal. The isoplanatic is defined as follows [8]:

$$\theta_0 = \left[2.91 \left(\frac{2\pi}{\lambda} \right)^2 \sec(\gamma)^{8/3} \int C_n^2(h) h^{5/3} dh \right]^{-3/5}, \quad (5)$$

it takes into account the whole distortion of the wavefront (low and high order modes).

In order to decouple the contribution stemming from the tip-tilt modes (i.e those related to the beam wander effect), the tilt-isoplanatic angle or the isokinetic angle, is defined as the angle between two sources, at which one of them jitters with a magnitude of half of its diffraction-limited divergence, with respect to the other one [10]:

$$\theta_{TA} = \frac{0.184 \lambda D^{1/6}}{[\sec(\gamma)^3 \int C_n^2(h) h^2 dh]^{1/2}} \quad (6)$$

Observe that the isokinetic angle depends on the zenith angle, the operating wavelength as well as the diameter of the receiver D . Therefore, working at large wavelengths and with large receiver apertures, allows to increase the isokinetic angle. Note that the contribution of the low-order modes (tip-tilt) accounts for $\approx 85\%$ of the total mean-square wavefront error, and that the low-order modes have effectively larger isoplanatic angle and decorrelation time than higher modes.

The relationship between the isokinetic angle and the point-ahead angle is of prime importance for optical communications. Indeed, if the angular offset between the signal emitted by the ground station and the signal received from the satellite (i.e., the point-ahead angle) remains smaller than the isokinetic angle, the downlink signal can be used to pre-compensate the uplink signal.

From the previous definitions, it turns out that the challenge lies in increasing the diameter of the beam while actively pre-compensating the beam wander induced by the atmosphere.

3. TEST CAMPAIGN – MEASUREMENT SETUP

3.1. THE OPTICAL GROUND STATION

The test campaign was carried out in May 2018 at the ESA’s Optical Ground Station (OGS) located at the “Observatorio del teide” at Izaña, in Tenerife. The site is located at an altitude of 2393 meters above sea level, well above the first inversion layer, and provides exceptional atmospheric conditions over long time periods throughout the year.

The telescope is a Zeiss 1m-diameter Ritchey-Chrétien telescope, supported by an English mount. It can be used in a Cassegrain or Coudé focus configuration. A 20 cm-diameter guider telescope, with a larger field of view, is fixed and co-aligned to the main telescope (Figure 1). The results presented in this paper have been obtained using the 1m-aperture telescope, with an Andor Ixon EMCCD camera fixed at the Cassegrain focus. The main parameters of the telescope and the camera are summarized in Table 1.



Figure 1: 1 meter Zeiss telescope of the OGS and 20 cm guider telescope.

Optical Ground Station (Ritchey–Chrétien Telescope)		Camera	
Location	Izaña (Tenerife)	Model	Andor Ixon EMCCD DV885KCS-VP
Geographic longitude	16° 30' 36.36" W	Calibration factor [arcsec/pixel]	0.124
Geographic latitude	28° 17' 58.29" N	Pixel size [μm^2]	8 x 8
Altitude above sea level [m]	2393	Frame rate [Hz]	150 to 250
Telescope diameter [mm]	1016	Exposure time [ms]	3 to 6
Cassegrain focus [m]	13.3	A/D resolution [bits]	16
Field of View [arcmin]	45		

Table 1: Main parameters of the telescope and the Andor camera.

3.2. ACQUISITION PARAMETERS

In the framework of this test campaign, only double stars with the following characteristics were considered for measurements: (i) a magnitude smaller than 8 (ideally 6), (ii) a magnitude difference smaller than 3 (ideally 2) and (iii) an angular separation between 4 and 60 arcseconds. Two optical filters have been used in front of the camera, one low-pass filter and one high pass-filter, to limit the optical spectrum to a range between 550 nm and 650 nm.

Given the focal length of the telescope, 13.3 meters, and the pixel size of the Andor camera, $8 \times 8 \mu\text{m}^2$, it turns out that the plate scale corresponds to 0.124 arcsec/pixel. Obviously, the smaller the plate scale, the higher the resolution, and the better the centroiding algorithm will perform. On the other hand, a high resolution involves a large number of pixels to process, which in turn limits the acquisition frequency.

Each double star measurement consisted of a sequence of 10 000 short exposures frames. The integration time was set between 3 ms and 6 ms per frame depending on the star magnitude, which is well below typical tip-tilt coherence time (> 10 ms) and long enough to reach an acceptable SNR. Therefore, the acquisition time of each 10 000-frames sequence lies between 30 and 60 seconds. The recording time of the entire sequence was chosen short enough that the statistical properties of the motion remain constant. Indeed, under typical conditions, the atmosphere is considered to maintain the same statistical properties for about 1 minute.

4. TILT ERROR DUE TO ANISOPLANATISM

A number of measurements were performed during the test campaign, but only part of them have been processed for the time being. This section first explains the data selection approach, and the centroiding method that was used to process the data. Then, the first experimental results are presented and compared to the analytical predictions.

4.1. DATA SELECTION

As a first step, all measurements were presented on a map according to the elevation and angular separation of the double stars. Then, four sets of double stars were identified for post-processing. The selection was based on the following criteria: (i) the possibility to deduce a trend from a given set, and (ii) the amount of data available during the same night. This map is presented on Figure 2. For the sake of clarity, Table 2 and Table 3 give another presentation of the same information. Before processing the data, a visual inspection of each selected sequence was performed individually in order to discard the sequences that were not relevant or too noisy. Note that most of the measurements were performed several times within a short time interval (i.e several minutes). This allows to check the repeatability of the measurement as well as the accuracy of the centroiding algorithm. This also gives an indication of the atmosphere's stability within a short time interval.

At the time of writing this paper, 63 sequences have been post-processed: 36 sequences to determine the impact of the elevation on the tilt anisoplanatism; 20 sequences to determine the impact of the angular separation of the double stars on the tilt anisoplanatism, and 7 sequences to evaluate the jitter of the telescope.

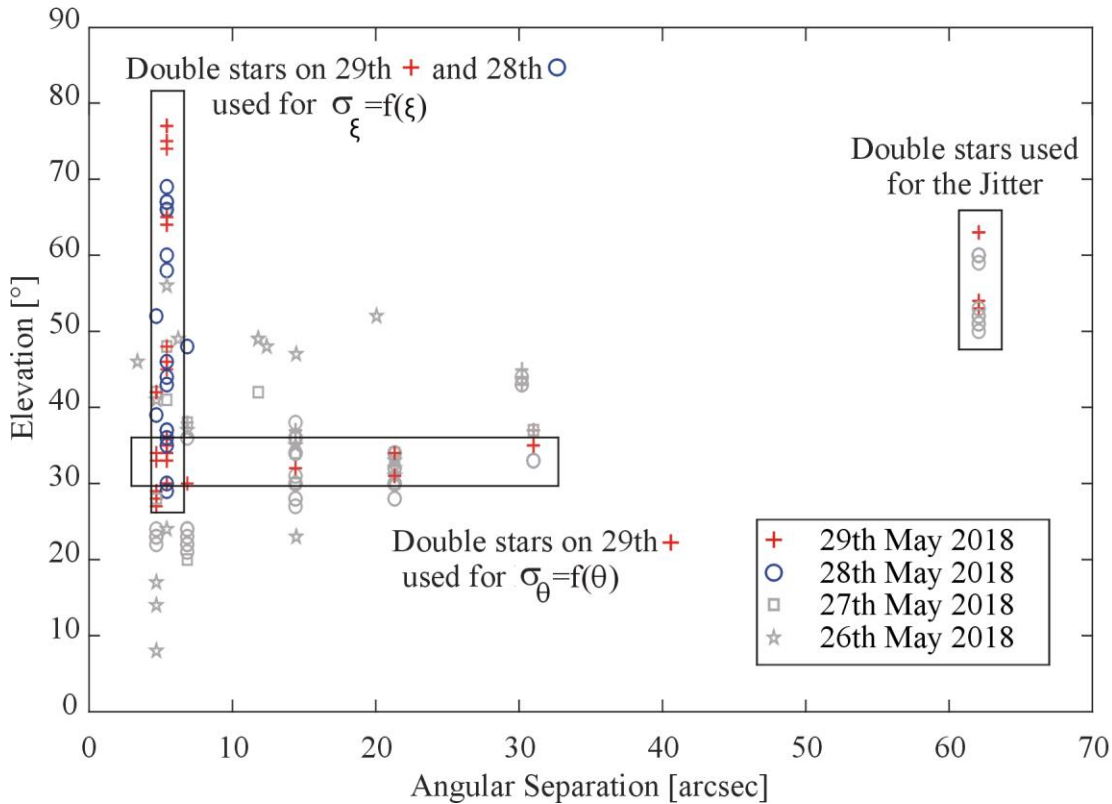


Figure 2: Map of the measurements that were performed on 26th, 27th, 28th and 29th of May 2018. The gray symbols have not yet been processed. Three rectangles show the group identified for analysis. Note that most of the measurements were performed several times (therefore they are superimposed on the map). The measurements are listed in Table 2, Table 3 and Table 4.

Double Star HIP 71762 : 5.42 "angular separation													
Right ascension (2000.0): 14 ^h 40 ^m 43.58 ^s							Declination (2000.0) :16°25'6.2"						
Date : 28 th May 2018, 00h00 to 6 am													
Elevation (°)	29 ¹	30 ¹	35 ¹	36 ¹	37 ²	43 ¹	44 ¹	46 ¹	58 ¹	60 ¹	66 ¹	67 ²	69 ¹
Date : 29 th May 2018, 00h00 to 6 am													
Elevation (°)	30 ²	33 ²	34 ²	35 ²	36 ²	45 ¹	46 ¹	48 ¹	64 ²	65 ²	74 ¹	75 ²	77 ¹

Table 2: 36 measurements of the double stars HIP 71762 were performed at different elevations. The superscript index indicate the number of measurements for a given elevation. The evolution of the tilt anisoplanatism with respect to the elevation is presented on Figure 6 a).

Date : 29 th May 2018, 00h00 to 6 am				
Double Star	Elevation [°]	Angular Separation [arcsec]	Right ascension (2000.0)	Declination (2000.0)
41 LEO ¹	33	4.69	10 ^h 08 ^m 22 ^s	11°58'2.9''
41 LEO ¹	34	4.69	10 ^h 08 ^m 22 ^s	11°58'2.9''
HIP 71762 ²	30	5.42	14 ^h 40 ^m 43.58 ^s	16°25'6.2''
HIP 71762 ²	33	5.42	14 ^h 40 ^m 43.58 ^s	16°25'6.2''
HIP 71762 ²	34	5.42	14 ^h 40 ^m 43.58 ^s	16°25'6.2''
HIP 71762 ²	35	5.42	14 ^h 40 ^m 43.58 ^s	16°25'6.2''
HIP 59832 ³	32	14.4	12 ^h 16 ^m 8.39 ^s	80°07'19.1''
HIP 62572 ²	31	21.318	12 ^h 49 ^m 13.4 ^s	83°24'46''
HIP 62572 ²	34	21.318	12 ^h 49 ^m 13.4 ^s	83°24'46''
HIP 75809 ³	34	31	15 ^h 29 ^m 9.98 ^s	80°26'58.2''

Table 3: 20 measurements of double featuring an angular separations between 4.69 arcseconds and 31 arcseconds were performed (at an almost constant elevation). The superscript index indicate the number of measurements for the same double stars. The evolution of the tilt anisoplanatism with respect to the angular separation is presented on Figure 6 b).

4.2. CENTROIDDING METHOD

The binarization is the first step of the centroiding process. It consists of applying a threshold on each frame of a given sequence in order turn the gray-scale image (encoded on 16 bits) into a binary image (i.e a mask). The mask is then applied on the initial frame as shown on Figure 3. This operation makes it possible to generate a new image where the background around the star is rejected.



Figure 3: a) The initial frame, b) after thresholding, the gray-scale image is turned into a binary image, c) result of the multiplication of a) with b).

Particular care must be taken when choosing the threshold as an inadequate value may lead to a wrong result. Under-estimating the threshold will generally not reject most of the background of the frame, whereas over-estimating the threshold may lead to an unphysical segmentation of a star in a number of independent areas. These scenarios are illustrated hereafter. Figure 4 a) presents the initial frame; Figure 4 b) shows the outcome of the algorithm when a (low) threshold of 970 and 975 are applied to the initial frame. From Figure 4 b), the following can be observed: (i) the algorithm cannot find the stars, and (ii) the result is strongly impacted by a very small change of the threshold value. Figure 4 c) shows a proper choice of the threshold value, the stars are well identified. Finally, Figure 4 d) presents a case where, one of the star is truncated, because the threshold is too large, which obviously leads to the wrong estimation of the center of gravity (CoG).

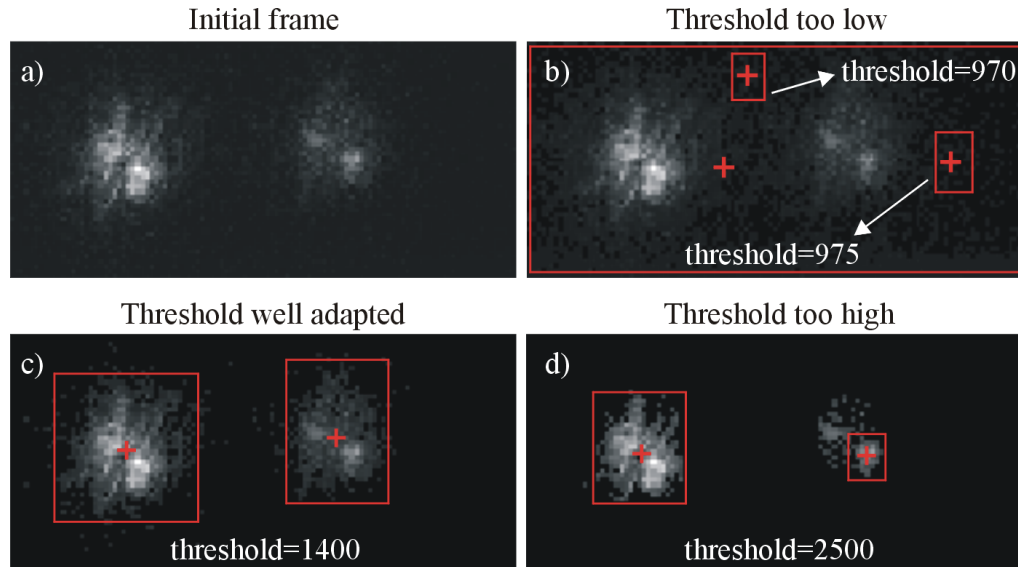


Figure 4: a) Initial frame; b) two different thresholds are applied: 970 and 975. The red rectangles show the four areas identified by the algorithm (one per star and per threshold). The largest rectangle is similar for both thresholds (the crosses are superimposed). If the threshold passes from 970 to 975, the algorithm gives a very different result; c) the algorithm converges, it identifies correctly the stars; d) the threshold is too high, one of the stars is over-segmented.

For a given threshold, one can easily find, for each frame of the sequence, the intensity-weighted centroid, as follow:

$$\begin{cases} x_c = \frac{\sum_{x=1}^m \sum_{y=1}^n I(x, y)x}{\sum_{x=1}^m \sum_{y=1}^n I(x, y)} \\ y_c = \frac{\sum_{x=1}^m \sum_{y=1}^n I(x, y)y}{\sum_{x=1}^m \sum_{y=1}^n I(x, y)} \end{cases} \quad (7)$$

where m and n stand for the size of the region (in pixels), respectively in the x and y directions. Note that the intensity-weighted method is the most commonly used, but other centroiding algorithm could be defined. As an example one can quote the so-called “squared weighting centroid method” where the intensity of each pixel is squared in the double sum [9].

Once the centroid of each star is identified, it is straightforward to deduce the distance between them, as well as the standard deviation of the distance, calculated over the entire sequence. It is worthwhile to point out that, because it is a differential method, the double star relative motion is inherently independent on the jitter of the telescope.

From the foregoing discussion, follows that the estimation of the CoG depends on the applied threshold. In order to have reliable results, the standard deviation of the distance between the two stars (i.e between their CoG) should be independent of the value of threshold. In fact, it has been observed that between those extreme “threshold-forbidden” regions, one can find a stable region where the standard deviation is constant, regardless the applied threshold. As an example, Figure 5 shows the evolution of the standard deviation with respect to the threshold, for a given sequence. One can clearly identify the region where the position of the centroid is impacted by the noise of the frame (the left part of the plot). Similarly, on the right hand side of the plot, the region associated with the over-segmentation of the stars is identified, which results in a divergence of the standard deviation. A stable region which does not depend on the threshold, is found between the two extremes previously identified. Note that (i) in some cases ($\approx 2\%$), no convergence has been found, in which case the sequence has been discarded, (ii) a frame containing at least one saturated pixel was systematically rejected and (iii) the method has been found very robust with regard to the number of frames considered in the sample. Indeed, thanks to the

large number of frames, keeping only 10% of them gives a very good approximation (i.e >90% accuracy) of the standard deviation determined over the entire sequence.

A curve similar to that presented on Figure 5 was generated for each sequence, making it possible to determine the threshold that is required as an input for the centroiding algorithm. Note that for a given sequence, the threshold was kept identical over all the frames.

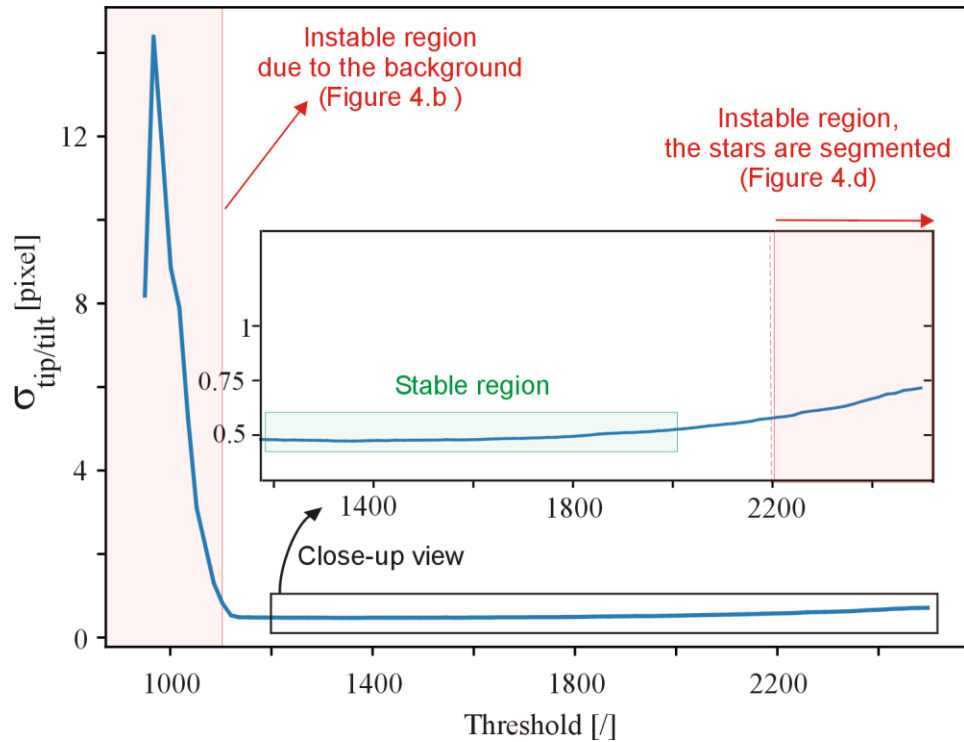


Figure 5: Evolution of the standard deviation of the relative motion, with respect to the threshold. The algorithm converges once the threshold is higher than the background. A stable region is found between ≈ 1200 and ≈ 1900 . If the threshold is too high, the algorithm may diverge.

4.3. ONE-AXIS RMS TILT CORRELATION

To a good approximation, the atmospheric turbulence may be seen as a static shape that is transported by the wind through the aperture of the telescope. This approximation is called the Taylor's frozen-atmosphere approximation. According to this model, the uncompensated atmosphere introduces a one-axis rms tilt error, given by the following equation [10]:

$$\sigma_{tilt} = 0.427 \frac{\lambda}{D} \left(\frac{D}{r_0} \right)^{5/6} \quad (8)$$

If the wavefront tilt measured in a given line of sight is used to estimate the tilt in another direction, then the one-axis rms tilt error that is due to anisoplanatism is given by [11] [12] :

$$\begin{cases} \sigma_{TA;x} = \{2[1 - C_x(\theta)]\}^{1/2} \sigma_{tilt} \\ \sigma_{TA;y} = \{2[1 - C_y(\theta)]\}^{1/2} \sigma_{tilt} \end{cases} \quad (9)$$

where $C_x(\theta)$ and $C_y(\theta)$ are the correlations of the tilts at two points that are separated by an angular distance θ . The x axis is parallel to the line joining the two stars, whereas the y axis is perpendicular to this line and characterizes the transverse relative motion. Squaring $\sigma_{TA;x}$ and $\sigma_{TA;y}$ and averaging gives a useful single measure of the one-axis rms tilt error that is due to tilt anisoplanatism:

$$\sigma_{TA} = [2 - C_x(\theta) - C_y(\theta)]^{1/2} \sigma_{tilt} \quad (10)$$

The correlation functions are given by:

$$C_{x,y}(\theta) = \frac{\int_0^\infty [A_0(s) \mp A_2(s)] C_n^2(h) dh}{\int_0^\infty C_n^2(h) dh},$$

$$\text{with } A_{0,2}(s) = \int_0^\infty [J_2(u)]^2 J_{0,2}(2su) u^{-14/3} du \quad (11)$$

$$\text{and } s = \frac{h \sec(\gamma) \theta}{D},$$

where the x and y indices in $C_{x,y}(\theta)$ respectively refer to - and + sign in the integral.

Numerical approximations of $A_{0,2}(s)$, with less than 0.2% error, can be calculated by the following [11] [12]:

$$A_0(s) = \begin{cases} \exp(-0.5866 s^{1.759}) & \text{for } 0 \leq s \leq 0.55 \\ 0.6656 s^{-1/3} [1 + 1/(6^3 s^2)] & \text{for } s > 0.55 \end{cases} \quad (12)$$

$$A_2(s) = \begin{cases} \exp(-1.941 s^{-0.4602}) & \text{for } 0 \leq s \leq 0.625 \\ 0.1331 s^{-1/3} [1 - 1/(6s^2)] & \text{for } s > 0.625 \end{cases} \quad (13)$$

By combining Eqs. (1), (3) and (8) to (13), it is possible to deduce, if not an exact value, at least an order of magnitude of the rms tilt error that is due to tilt anisoplanatism. Furthermore, its evolution with respect to the elevation, σ_ξ , and with regard to the angular separation between the double stars, σ_θ , can also be determined. The following section compares the numerical simulations of the rms tilt error due to tilt anisoplanatism to the experimental results obtained with the centroiding algorithm.

4.4. PRELIMINARY RESULTS

Figure 6 a) shows the numerical prediction and an experimental measure of the rms tilt error due to anisoplanatism, for various elevations of the double stars HIP 71762 (featuring an angular separation of 5.42 arcseconds). The measurements were performed between 00h00 and 6h am, on the 28th and 29th of May (all the measurements are listed in Table 2). One observes that the experimental results are in very good agreement with the numerical simulations for both days. However, even though the experimental values are very close to the numerical prediction, the figure suggests, an overestimation of the model (or an underestimation of the experimental results) for elevations smaller than 30°. Of course, this discrepancy

can also stem from a change in the atmospheric turbulence over the night. Unfortunately, it has not been possible to recover the instantaneous atmospheric parameters for these days. Therefore, $r_0(\gamma)$ was determined by means of Eq. (3).

Figure 6 b) presents the experimental measure of the rms tilt error due to anisoplanatism, for a fixed elevation of $\approx 32^\circ$ and several angular separations (listed in Table 3). The measurements are compared to the numerical prediction for $r_0 = 10\text{ cm}$, $r_0 = 15\text{ cm}$ and $r_0 = 20\text{ cm}$ (note that the value predicted by Eq.(3) is $r_0 = 16.2\text{ cm}$ at this elevation). The experimental results are still clearly in the same order of magnitude as the theoretical model, and in the same way as for Figure 6 a), overestimated by the model at such a low elevation. The discrepancy may indicate the modified HV model described by Eq. (1) overestimates the altitude of the turbulent layer. It is, however, interesting to note that the numerical model follow a trend similar to that measured experimentally.

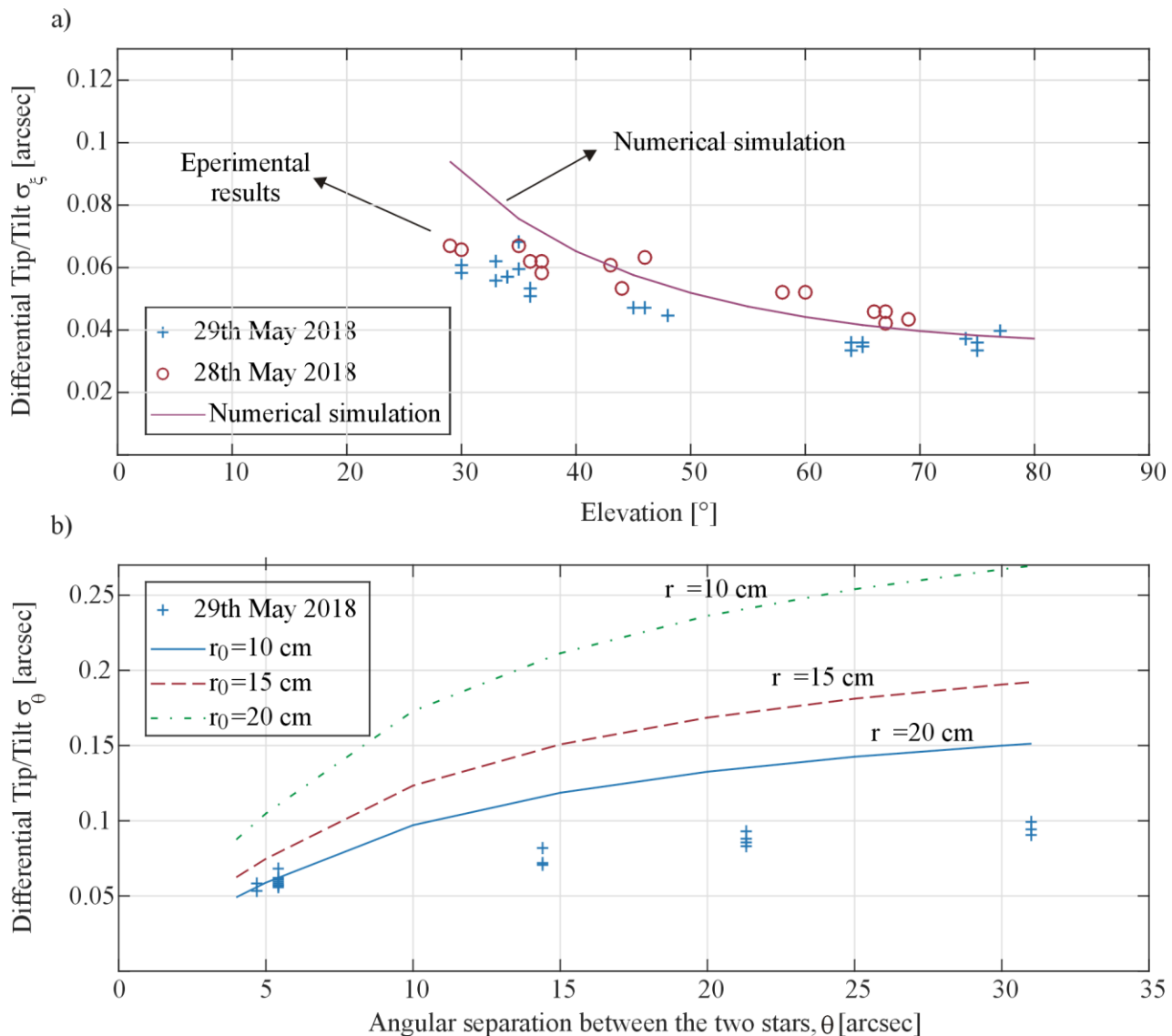


Figure 6: a) Evolution of the rms error due to tilt anisoplanatism, for various elevations (the angular separation is 5.42 arcseconds). The measurements were performed on 29th and 28th of May 2018 between 00h00 and 6 am (see Table 2). b) Evolution of the rms error due to tilt anisoplanatism, for various angular separations (the elevation is about 32°) and for three values of r_0 (note that the value predicted by Eq.(3) is $r_0 = 16.2\text{ cm}$ at this elevation). The measurements were performed on 29th of May 2018 between 00h00 and 6 am (see Table 3).

It is important to mention that even though the tilt contribution statistically account for $\approx 85\%$ of the full rms error, the experimental measurements, acquired with the 1m telescope, also suffer from higher-order aberrations. Conversely, the numerical predictions have been performed considering only the tilt contribution of the full error due to anisoplanatism. Therefore, a more representative measurement should be performed with the smaller 20 cm aperture telescope, over which the wavefront could be considered as almost coherent. However, the amount of photons gathered by the telescope would be 25 times smaller than with the 1m telescope. An alternative lies in increasing the operating wavelength. Indeed, according to Eq. (8), the tilt should remain unchanged, while the Fried parameter should increase proportionally to $\lambda^{6/5}$ as shown by Eq. (3).

5. JITTER

Besides the turbulence-induced beam wander discussed in the previous section, another issue of concern arises from the jitter that may be experienced by the uplink beam, as a result of the vibrations of the ground station. These pointing errors can stem from the flexible motion (or rigid-body motion) of the telescope structure excited by the wind, from residual vibrations after the tracking of a target, from vibrations of machines fixed on the telescope, etc. This section shows how the jitter of the telescope can be estimated using two stars separated with an angle large enough to be considered as statistically independent. For the sake of simplicity, one consider only the jitter in one direction, x axis, but, obviously, the same reasoning holds for the y axis.

One first notes that the variance of the centre of gravity of the double stars system, $Var(\text{CoG}_x)$, has two independent contributions: one arising from the jitter of the telescope, $Var(\text{CoG}_x)|_{seeing=0}$, and one from the seeing, $Var(\text{CoG}_x)|_{J_x=0}$:

$$Var(\text{CoG}_x) = Var(\text{CoG}_x)|_{seeing=0} + Var(\text{CoG}_x)|_{J_x=0} \quad (14)$$

JITTER = 0 AND SEEING \neq 0

The properties of the variance allow to write:

$$Var(\text{CoG}_x)|_{J_x=0} = Var\left(\frac{x_1 + x_2}{2}\right) = \frac{1}{4}[Var(x_1) + Var(x_2)] = \frac{1}{4}[Var(x_1 - x_2)] = \frac{1}{4}[Var(\Delta x)] \quad (15)$$

where x_1 and x_2 stand for the absolute coordinate of star 1 and 2 with respect to a given coordinate system.

JITTER \neq 0 AND SEEING = 0

If there is no seeing, the motion of the center of gravity is due to the jitter:

$$Var(\text{CoG}_x)|_{seeing=0} \equiv Var(J_x) \quad (16)$$

Therefore, one can write:

$$Var(\text{CoG}_x) = Var(\text{CoG}_x)|_{seeing=0} + Var(\text{CoG}_x)|_{J_x=0} = Var(J_x) + \frac{1}{4}[Var(\Delta x)] \quad (17)$$

And one directly deduces the jitter of the telescope:

$$Var(J_x) = Var(\text{CoG}_x) - \frac{1}{4}[Var(\Delta x)] \quad (18)$$

The measurements were performed a first time around 2h00 am, and a second time around 4h00 am on 29th of May. The results are given in Table 4. One can see that the jitter is larger at 2h00 am. This can be due to a change of the wind velocity, or to a variation of the jitter with respect to the position of the telescope.

The results confirm the excellent pointing and tracking stability performances of the ESA's OGS telescope, i.e., <0.5 arcsec.

Double Star HIP 85819 :62 "angular separation							
Right ascension (2000.0): 17 ^h 32 ^m 10.72 ^s				Declination (2000.0): 55°11'4.1"			
Elevation [°]	σ_{CoG_x} [arcsec]	σ_{CoG_y} [arcsec]	σ_{Δ_x} [arcsec]	σ_{Δ_y} [arcsec]	σ_{J_x} [arcsec]	σ_{J_y} [arcsec]	Time
53	0.27	0.35	0.11	0.10	<u>0.27</u>	<u>0.35</u>	01h54 am
54	0.35	0.36	0.10	0.09	<u>0.35</u>	<u>0.36</u>	01h59 am
54 _b	0.30	0.30	0.09	0.08	<u>0.30</u>	<u>0.30</u>	02h05 am
63	0.24	0.15	0.08	0.06	<u>0.24</u>	<u>0.15</u>	04h00 am
63 _b	0.21	0.19	0.08	0.06	<u>0.20</u>	<u>0.19</u>	04h03 am
63 _c	0.17	0.16	0.07	0.08	<u>0.17</u>	<u>0.15</u>	04h05 am
63 _d	0.23	0.20	0.10	0.07	<u>0.23</u>	<u>0.19</u>	04h07 am

Table 4: 7 measurements were performed on 29th May 2018 to estimate the jitter of the telescope.

6. DIMENSIONING OF THE GROUND-BASED TRANSMITTER APERTURE DIAMETER

In this section, a methodology is proposed to determine the maximum transmitter aperture diameter of a ground-based laser communication terminal, such that tip-tilt pre-compensation based on the received satellite signal, can still be successfully applied to the uplink beam.

The pointing direction of the uplink laser signal transmitted by an optical ground station is calculated based on (i) the direction of the received downlink signal from the satellite and (ii) the point-ahead angle. As long as the point-ahead angle is below the tilt-isoplanatic angle or the isokinetic angle, this computation is sufficiently accurate to effectively illuminate the satellite with the uplink beam. The larger the ground-based transmitter aperture, the smaller the uplink divergence, and therefore, the more accurate the estimation of the uplink direction needs to be in order to minimize the pointing loss.

Two scenarios are analysed: (i) GEO satellite case and (ii) LEO satellite case, both at 1064nm and 1550nm wavelengths. The point-ahead angle is typically ~4 arcsec (respectively ~10 arcsec) for the GEO scenario (respectively LEO scenario). Based on the results presented in Figure 6 b), one derives that the one-axis rms tilt error due to tilt anisoplanatism (i.e., differential tip-tilt value) for an angular separation ~4 arcsec (respectively ~10 arcsec) is around 0.07 arcsec (respectively 0.1 arcsec) during night-time conditions. Note that the measured values are taken instead of the theoretical values, as the intention is to dimension the ground-based transmitter at the specific location of the ESA's OGS. This methodology can be applied to other locations by using the site-specific differential tip-tilt measurements. The differential tip-tilt values at the ESA's OGS were measured with the 1m-diameter telescope. For a different aperture diameter, the extrapolated differential tip-tilt is proportional to $\sim D^{(-1/6)}$ law, as indicated by Eq.(8). This differential tip-tilt is an inherent source of miss-pointing (i.e., it cannot be corrected by tip-tilt pre-compensation), and effectively it introduces a pointing loss, which depends on the divergence angle of the ground-based transmitter aperture. This analysis assumes that the effective

transmitter aperture is not limited by the atmosphere (i.e., Fried parameter \gg transmitter aperture diameter). However, in reality, the uplink beam divergence is constraint by the minimum of the ground-based transmitter aperture diameter and the Fried parameter.

Figure 7 shows the pointing loss in the uplink direction induced by tilt anisoplanatism (selecting the measured values from Figure 6 (b), which were derived at an elevation angle $\approx 32^\circ$), taking into account the divergence angle of the ground-based transmitter. The calculations consider a maximum acceptable pointing loss of 3dB and a ground-based transmitter laser at 1064nm wavelength. For the LEO scenario, the maximum ground-based transmitter aperture diameter is ~ 20 cm assuming a differential tip-tilt of 3^* (measured) differential tip-tilt. Taking a factor x2 margin and 3^* rms value for the differential tip-tilt, the maximum ground-based transmitter aperture diameter reduces to ~ 9 cm. For the GEO case, the maximum ground-based transmitter aperture diameter is ~ 32 cm considering a differential tip-tilt of 3^* (measured) differential tip-tilt. Taking a factor x2 margin and 3^* rms value for the differential tip-tilt, the maximum ground-based transmitter aperture diameter reduces to ~ 14 cm.

Similar calculations are presented in Figure 8 but for a ground-based transmitter laser operating at 1550nm wavelength. For the LEO scenario, the maximum ground-based transmitter aperture diameter is ~ 33 cm assuming a differential tip-tilt of 3^* (measured) differential tip-tilt. Taking a factor x2 margin and 3^* rms value for the differential tip-tilt, the maximum ground-based transmitter aperture diameter reduces to ~ 14 cm. For the GEO case, the maximum ground-based transmitter aperture diameter is ~ 50 cm considering a differential tip-tilt of 3^* (measured) differential tip-tilt. Taking a factor x2 margin and 3^* rms value for the differential tip-tilt, the maximum ground-based transmitter aperture diameter reduces to ~ 22 cm.

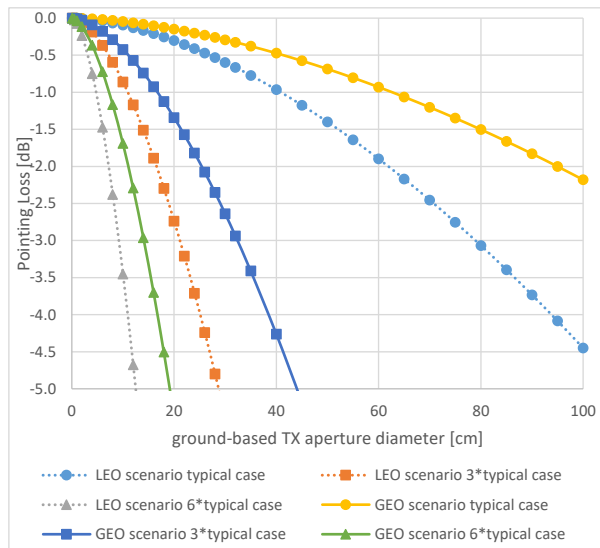


Figure 7. Pointing loss (in dB) as a function of the ground-based transmitter aperture diameter (in cm) due to residual differential tip-tilt. Solid lines (respectively dashed lines) correspond to GEO scenario (respectively LEO scenario). “Typical case” means one rms differential tip-tilt value is considered (values in Figure 6 b). Additionally, the curves for 3^* rms and 6^* rms values are depicted. The calculations assume a ground-based transmitter laser at 1064nm wavelength.

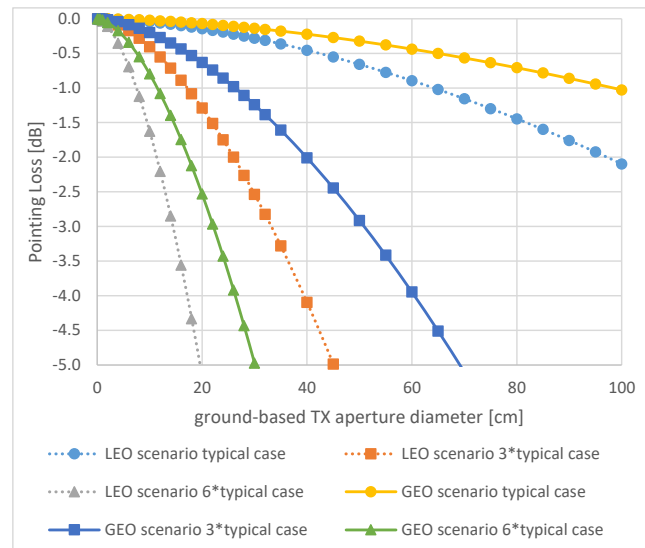


Figure 8. Pointing loss (in dB) as a function of the ground-based transmitter aperture diameter (in cm) due to residual differential tip-tilt. Solid lines (respectively dashed lines) correspond to GEO scenario (respectively LEO scenario). “Typical case” means one rms differential tip-tilt value is considered (values in Figure 6 b). Additionally, the curves for 3^* rms and 6^* rms values are included. The calculations assume a ground-based transmitter laser at 1550nm wavelength.

7. CONCLUSION

This paper reports on the results obtained from a test campaign carried out at the ESA's Optical Ground Station in May 2018. Double stars measurements have been performed for different angular separations and at various elevations. The goal is to evaluate the potential effect of tilt-anisoplanatism on an optical uplink pre-compensation based on the downlink signal.

First, a method aiming at extracting the relative motion (tip-tilt) of the double stars is described. Then, the experimental results are compared to a theoretical model (which is based on the modified Hufnagel-Valley model adapted to Tenerife). It turned out that the experimental results are in rather good agreement with the numerical predictions. More specifically, the order of magnitude of the experimental values is fully consistent with that obtained with the theoretical model (the numerical predictions are 2.5 higher than the experimental values for the worst case and a factor 1 is noticed in the best case). The trend of the measurements, with respect to the elevation and the angular separation, is also similar to that predicted by the model although a discrepancy is suggested, particularly at low elevations (i.e. $\approx 30^\circ$). Note, however, that the theoretical model may also be rather inaccurate since it does not account for instantaneous meteorological conditions or seasonal influences.

Even though the differential method used in this paper is inherently insensitive to the vibrations of the telescope, the jitter of the transmitter is of utmost importance for an uplink transmission. Section 5 presents a way to evaluate it, based on the measurements of double stars featuring a large angular separation (62 arcseconds). The results confirm exceptional pointing and tracking stability performances <0.5 arcsec rms. Note that the jitter could also be characterized (and possibly compensated) by means of accelerometers (placed along the tube of the telescope, on the back of the mirror, on the spider, and on the camera).

For the time being, only part of the measurements have been post-processed. Of course, concluding about the consistency of the experimental results with respect to a theoretical model requires further analysis (and more measurements). Other centroiding algorithms will be investigated as well. Besides this, other models may be used to predict the trend of the measurements (e.g. Izaña Day Model and the Izaña Night Model). As a future improvement, one could consider to use a smaller telescope (e.g. the 20 cm guider telescope), which would make it less sensitive to high-order wavefront distortions and would give a more representative evaluation of the tilt anisoplanatism; at the cost of a smaller amount of power received from the stars. This, however, can be faced by increasing the integration time which is well below the tip-tilt coherence time. As an alternative, one could increase the operating wavelength to near-infrared (instead of 600 nm). This would improve the Fried parameter, whereas the tip-tilt should be constant regardless of the wavelength.

Finally, a methodology to determine the maximum transmitter aperture diameter of a ground-based laser communication terminal, in case tip-tilt pre-compensation is applied to the uplink signal based on the received satellite signal, is thoroughly discussed. Available results indicate that tip-tilt pre-compensation can be successfully applied to the uplink beam for transmitter aperture diameters up to ~ 9 cm / ~ 14 cm (respectively at 1064nm / 1550nm wavelength) for the LEO scenario, and ~ 14 cm / ~ 22 cm (respectively at 1064nm / 1550nm wavelength) for the GEO scenario, taking into account tilt anisoplanatism effects due to the required point-ahead angle (3dB maximum pointing loss as criteria). These conclusions need to be confirmed by further test campaigns to cover elevation angles $<30^\circ$, daytime conditions and seasonal effects.

8. ACKNOWLEDGMENT

This study was supported by the European Space Agency (ESA) in the framework of the ARTES ScyLight programme. D. Alaluf was supported by the Belgian Federal Science Policy Office (BELSPO). The authors also gratefully acknowledge the Instituto de Astrofísica de Canarias (IAC) as well as the sky quality group (<http://www.iac.es>) for their support during the measurements campaign.

REFERENCES

- [1] H. Henniger, O. Wilfert, *An Introduction to Free-space Optical Communications*. Radioengineering, 19(2).
- [2] A. Belmonte, Taylor, M. T., Hollberg, L., & Kahn, J. M. (2017). *Effect of atmospheric anisoplanatism on earth-to-satellite time transfer over laser communication links*. Optics express, 25(14), 15676-15686, 2010
- [3] Mata-Calvo, R., Calia, D. B., Barrios, R., Centrone, M., Giggenbach, D., Lombardi, G., Becker, P., Zayer, I. *Laser guide stars for optical free-space communications*. In Free-Space Laser Communication and Atmospheric Propagation XXIX (Vol. 10096, p. 100960R). International Society for Optics and Photonics, February 2017.
- [4] Beland, R.R. *Propagation Through Atmospheric Optical Turbulence, in Atmospheric Propagation of Radiation*, Smith F.G., Ed.; The Infrared and Electro-Optical Systems Handbook, Vol. 2; SPIE Optical Engineering Press: Bellingham, WA, 1993.
- [5] Giggenbach, D., *Optimierung der optischen Freiraumkommunikation durch die turbulente Atmosphäre - FocalArray Receiver*, PhD thesis, Universität Der Bundeswehr München (November 2004).
- [6] Andrews, L. and Phillips, R., *Laser Beam Propagation through Random Media*, SPIE Press, 2nd edition ,2005.
- [7] D. L. Fried, *Optical resolution through a randomly inhomogeneous medium for very long and very short exposures*, J. Opt. Soc. Am. 56, 1372-1379 (1966).
- [8] Fried D.L., *Anisoplanatism in adaptive optics* , J. Opt. Soc. Amer. A., 72 , pp. 52-61, 1982
- [9] G. Zhang, *Processing of Star Catalog and Star Image*. In Star Identification (pp. 37-72). Springer, Berlin, Heidelberg, 2017.
- [10] R. J. Sasiela, *A unified approach to electromagnetic wave propagation in turbulence and the evaluation of multiparameter integrals*, Tech. Rep. 807 (MIT Lincoln Laboratory, Lexington, Mass., 1988.
- [11] G. C. Valley, *Isoplanatic degradation of tilt correction and short-term imaging systems*, Appl. Opt. 19, 574-577 1980.
- [12] S. S., Olivier, D. T., Gavel, *Tip-tilt compensation for astronomical imaging*. JOSA A, 11(1), 368-378, 1994.